Development and evaluation of matrix application techniques for high throughput mass spectrometry imaging of tissues in the clinic

Clinical Mass Spectrometry 12 (2019) 7–15

Contents lists available at ScienceDirect

Clinical Mass Spectrometry

journal homepage: www.elsevier.com/locate/clinms

Development and evaluation of matrix application techniques for high throughput mass spectrometry imaging of tissues in the clinic

Lennart R.S. Huizing[a], Shane R. Ellis[a], Bart W.A.M.M. Beulen[b], Florian P.Y. Barré[a], Paul B. Kwant[b], Rob J. Vreeken[a,c], Ron M.A. Heeren[a,*]

[a] The Maastricht MultiModal Molecular Imaging Institute (M4I), Division of Imaging Mass Spectrometry, Maastricht University, Universiteitssingel 50, 6229 ER Maastricht, The Netherlands

[b] Instrument Development Engineering and Evaluation, Engineering Department, Maastricht University, Universiteitssingel 50, 6229 ER Maastricht, The Netherlands

[c] Janssen R&D, Turnhoutseweg 30, 2340 Beerse, Belgium

ABSTRACT

Matrix-assisted laser desorption ionization (MALDI) mass spectrometry imaging (MSI) is a sensitive label-free technique that can be used to study a wide variety of clinical phenotypes. In this context, MSI offers huge diagnostic potential by supporting decision making in the determination of personalized treatment strategies. However, improvements in throughput and robustness are still needed before it finds a place in routine application. While the field has seen tremendous improvements in the throughput of data acquisition, robust and high-throughput sample preparation methods compatible with these acquisition methods need to be developed. To address this challenge, we have developed several methods to reduce the matrix application time to less than 5 min, while maintaining sensitivity and reproducibility. Workflows incorporating these methods provide a pipeline analysis time for MSI sample preparation and acquisition of less than 30 min. The reduced time for these analyses will contribute towards the integration of MSI into routine molecular pathology for clinical diagnostics.

1. Introduction

Matrix-assisted laser desorption ionization (MALDI) mass spectrometry imaging (MSI) provides a technique for molecular characterization, diagnosis and classification of tissues in a spatially resolved manner for various diseases (e.g., non-alcoholic fatty liver disease, infectious disease and cancer) [1–4]. For cancer, MALDI-MSI has been used to classify tumours and to visualize inter- and intra-tumour molecular heterogeneity [1,5–9], which may lead to either different treatment responses or tumor persistence and recurrence, despite initially successful chemotherapy [1,10]. These cases indicate that detailed characterization of a tumor's molecular composition could contribute to increased diagnostic accuracy, increased precision of treatment, increased prognostic confidence, and, subsequently, increased frequency of positive outcomes.

For MALDI-MSI to mature into a routine clinical diagnostic tool, with utility in large-scale clinical and pharmaceutical research [11–14], it will be necessary that it support a rapid, reproducible and sensitive workflow. The recent arrival of commercially available high-speed, high-spatial resolution, imaging mass spectrometers brings MSI closer to routine clinical diagnostics [15–17]. This resultant increase in measurement speed led us to investigate more steps in the workflow, particularly the sample preparation methods, to provide optimal compatibility with high-throughput MSI workflows. Matrix application, in addition to sectioning, mounting and drying the tissue, are the primary time-consuming aspects of sample preparation for MSI. The matrix needs to form a homogeneous layer on the tissue to ensure that detected differences accurately reflect molecular content rather than matrix layer variation. Additionally, analyte delocalization, caused by solvation and spreading of molecular entities by the solvent in the matrix before crystallization, should be minimized to retain the spatial features of the tissue [18]. Hence, it is vital to develop standardized and rapid

Abbreviations: CHCl3, chloroform; Da, Dalton; DHB, 2 5-dihydroxybenzoic acid; e.g, exempli gratiā; FT-ICR, Fourier transform ion cyclotron resonance; FT-MS, Fourier transform mass spectrometry; FWHM, full width at half maximum; H&E, hematoxylin and eosin; i.e, id es; ITO, indium tin oxide; *m/z*, mass over charge ratio; MALDI, matrix assisted laser desorption ionization; mBar, milliBar; MeOH, methanol; MSI, mass spectrometry imaging; NRM, norharmane; Pa, Pascal; PC, phosphatidylcholine; PE, phosphatidylethanolamine; PI, phosphatidylinositol; Ppm, parts per million; RSD, relative standard deviation; S/N, signal-to-noise ratio; SM, sphingomyelin; TFA, trifluoroacetic acid; TIC, total ion count; TOF, time-of-flight; V:V, volume concentration

* Corresponding author.

E-mail address: r.heeren@maastrichtuniversity.nl (R.M.A. Heeren).

https://doi.org/10.1016/j.clinms.2019.01.004

Received 12 July 2018; Received in revised form 27 January 2019; Accepted 28 January 2019

Available online 28 January 2019

matrix application methods that will provide reliable, sensitive and reproducible results for MSI to be applicable in clinical diagnostics and pharmaceutical studies.

At present, the most common approach for matrix-application employs an automated sprayer. Most automated matrix sprayers nebulize the matrix solution while moving at a constant speed over the tissue, thereby depositing a thin matrix layer [19–22]. While automated sprayers have significantly improved reproducibility, the spatial resolution of MSI can still be limited by large (e.g., low- to mid-micrometer) crystal formations and the possibility of analyte delocalization caused by the solvent [23–25]. Although recent papers show improvement in spray-based coating methods [25–27], the need to apply several layers of matrix, to ensure a homogenous and sufficiently thick coating, can still take a considerable amount of time (over 20 min per slide).

Matrix sublimation, an alternative to matrix spraying, is a dry, solvent-free, matrix-application procedure [23,28–31]. For matrix sublimation, both sample and matrix are placed in a vacuum and the matrix is heated at reduced pressure resulting in its sublimation (i.e., a direct solid-vapour phase transition). The gaseous matrix then condenses onto the sample, which has been cooled, typically with water or ice sludge [28]. Sublimation results in a homogenous coating of high-nanometer- to low-micrometer-sized crystals on the target sample. These smaller, homogenously deposited crystals, in combination with a reduced risk of delocalization due to the absence of solvent wetting, facilitate higher spatial resolution imaging by preserving molecular distributions on a smaller scale [24,29,32]. Besides, only a few minutes are required to properly cover a sample using sublimation, which makes sublimation more amenable for high-throughput workflows [33].On the other hand, the lack of solvents in the method can result in less efficient extraction of certain molecules into the matrix [24,34]. Although this effect appears to be minimal for lipids, at least, and can be partially overcome for other molecular classes by recrystallization of the sublimated matrix or spraying additional matrix after sublimation, this would obviously involve extra steps that could limit the high-throughput compatibility of the technique [34,35].

Here, we evaluated both sublimation and spraying, as rapid means of matrix application for lipid imaging of biological tissues, with the goal of achieving complete sample preparation within 30 min for potential clinical use in high-throughput MALDI-MSI [36,37]. The matrices 2,5-dihydroxybenzoic acid (DHB) and norharmane (NRM, 9H-Pyrido[3,4-b]indole) were tested in both positive and negative ion mode. Process aspects that were measured and evaluated were: sample preparation speed, reproducibility of number of spectral peaks, signal intensity, and analyte delocalization.

2. Materials and methods

2.1. Chemicals

All matrices were purchased from Sigma-Aldrich (Zwijndrecht, The Netherlands). Solvents were obtained from Biosolve bv (Valkenswaard, The Netherlands). All solvents used were HPLC grade or better.

2.2. Tissue

Mini pig colons were snap-frozen and stored at −80 °C. Tissue cryosections of 12 µm thickness were cut using a cryomicrotome (HM525 Microm, Walldorf, Germany) and mounted on indium tin-oxide (ITO) coated glass slides (Delta Technologies, Loveland, CO, USA). All studies were approved by the local animal ethical committee and all studies were conducted in facilities accredited by national institutions adhering to AALAC guidelines. In line with standard procedures for matrix spraying, samples were desiccated in a vacuum desiccator for 20 min prior to matrix coating, unless stated otherwise. To evaluate elimination of this time-costly vacuum desiccation step, some samples were not desiccated prior to matrix sublimation, or were desiccated with nitrogen gas prior to matrix spraying.

2.3. Matrix application

Matrix application methods were developed and tested at a 100 µm raster size. Matrix was sprayed onto tissue samples using a SunCollect (SunChrom, Friedrischsdorf, Germany) automated sprayer or a TM-Sprayer (HTX-Technologies, Chapel Hill, North Carolina, USA). Spraying methods were optimized to allow sufficient matrix deposition within 10 min whilst minimizing delocalization and maintaining a good average signal-to-noise ratio (S/N > 15).

DHB was dissolved at 40 mg/ml in 1:1 $CHCl_3$:MeOH (V:V) with 0.2% trifluoroacetic acid (TFA) and NRM was dissolved at 30 mg/ml in 2:1 $CHCl_3$:MeOH (V:V). Matrix was sonicated (~10 min) to prevent remaining matrix crystals from clogging the tubing in the spraying system. Spray settings are shown in Supplementary Table 1.

Sublimation was performed using an in-house built sublimation apparatus (Fig. S1). An amount of 80 mg of DHB or NRM matrix dissolved in acetone was placed onto a heating plate for each run. Prior to adding the matrix, the heating element was preheated to 60 °C. The matrix solution was allowed to rapidly evaporate on the heating plate with the goal of achieving maximum contact between the matrix and the heating element to enhance the sublimation efficiency. The sample-holder was actively cooled with flowing tap water and the sample was attached with two metal clips in effort to achieve the highest possible contact between the sample and the cooled holder. Pressure in the sublimation chamber was stabilized at approximately 2.0×10^{-2} mBar (2 Pa) prior to heating the matrix (~1 min). The sublimation temperature was set to 160 °C for DHB and 140 °C for NRM. DHB was sublimated for 160 s and NRM was sublimated for 180 s.

2.4. MALDI-MSI measurements

High throughput imaging measurements were performed on the rapifleX MALDI Tissuetyper™ (Bruker Daltonik GmbH, Bremen, Germany) in reflectron mode at a 100 µm, 50 µm or 10 µm raster size. DHB was measured in positive ion mode, NRM was measured in first positive and, subsequently, negative ion mode. Dual polarity images were obtained, as previously described [15]. To test signal intensity, the number of peaks and reproducibility of samples were measured at 100 µm, rather than 50 µm, raster to reduce the time of analysis and, thereby, any correlated loss of signal due to evaporation of matrix in the mass spectrometer. The three coating methods, sublimation, SunCollect, and TM-Sprayer, were measured on the same slide in effort to minimize differences in analysis conditions; for this, two of the sections were covered with aluminium foil during the matrix application process. The measurements were performed in triplicate on consecutive sections. For each measurement group, the order was changed in which each matrix application method was analyzed to control for potential signal loss due to matrix evaporation in the mass spectrometer. 50 µm and 10 µm raster size images were each measured individually. Samples were measured at a mass range between 200–2000 m/z for NRM and 260–2000 m/z for DHB (increased minimum for DHB because matrix interference peaks dominated the spectrum). An area away from tissue was analyzed to collect data on peaks specific for each matrix. Data were visualized using FlexImaging software 5.0 (Bruker Daltonik GmbH, Bremen, Germany). Measurements were normalized to the total ion count (TIC) per pixel. Spectra were exported from FlexImaging as CSV files to Mmass [38] for peak picking to obtain information on the number of peaks and S/N per condition. To avoid sampling bias, the entire tissue was used to evaluate the number of peaks and the S/N. By using consecutive sections, all tissues had similar amounts of pixels, which was around 18,500 pixels per section. Peak picking settings in Mmass were set at a S/N threshold of 10, and the picking height was set at 43%. Both absolute and relative intensity threshold were set at 0. No

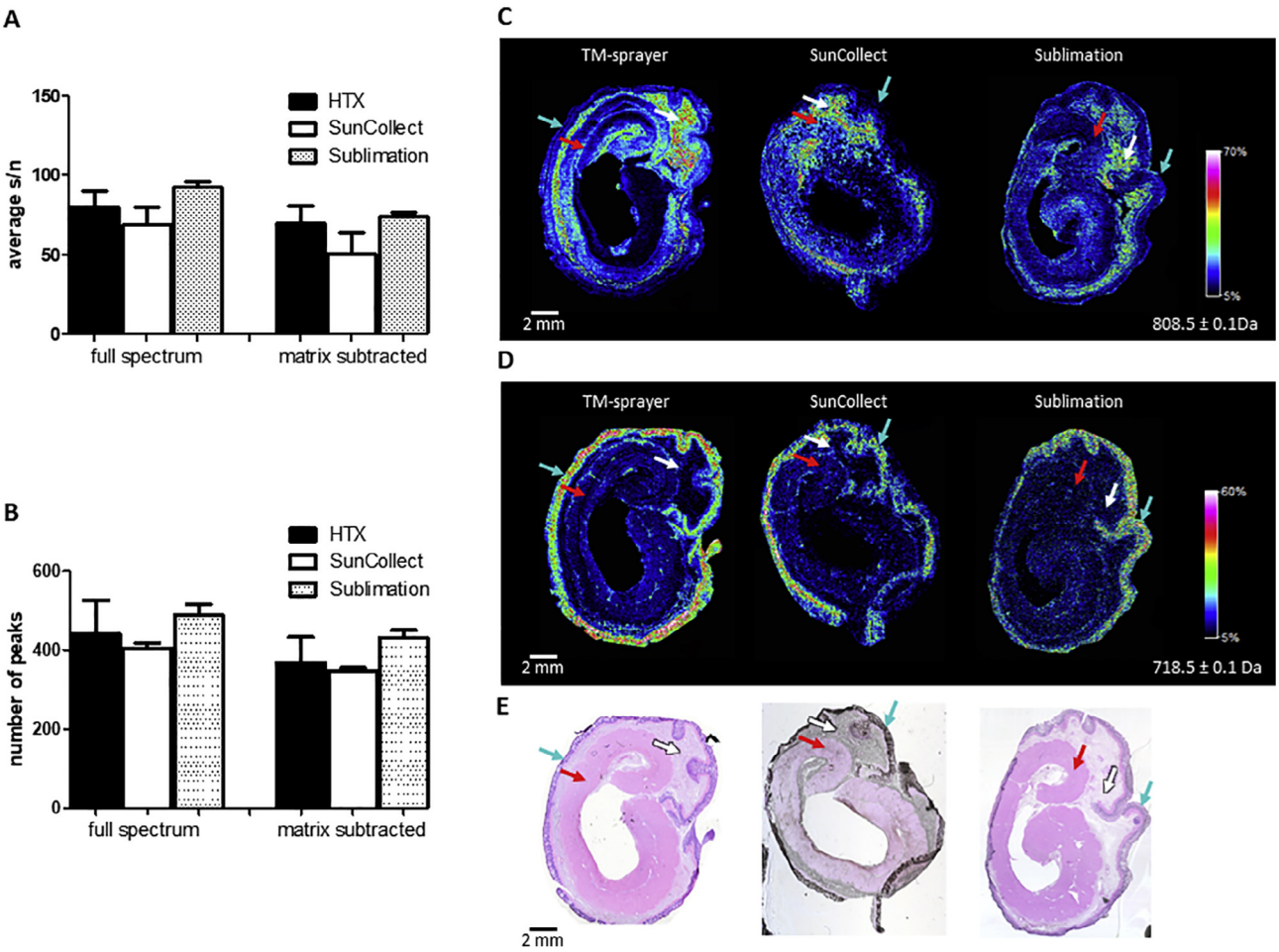

Fig. 1. Signal intensity (A, C, D) and detected peaks (B) in positive ion mode matrix application of NRM. (A) Average S/N obtained after matrix application using HTX, SunCollect or sublimation for the full spectrum (left bars) or after matrix peak were subtracted (right bars). Error bars represent standard deviation (n = 3). (B) Mean number of peaks obtained after matrix application using HTX, SunCollect or sublimation for the full spectrum (left bars) or after matrix peak were subtracted (right bars). Error bars represent standard deviation (n = 3). (C) Ion intensity distribution at 50 µm raster size of *m/z* 808.5 ± 0.1 Da ($[PC\ 36:2 + Na]^+$) and (D) 718.5 ± 0.1 Da $[PC\ O\text{-}32:1 + H]^+$. Images were normalized to TIC. (E) H&E stain of the measured tissues corresponding to the images in C and D. Arrows show mucosa (blue), submucosa (white), and muscle (red) on H&E and corresponding location in the *m/z* images.

baseline correction or smoothing was performed. Matrix-related peaks were subtracted from the tissue spectrum by subtracting the spectrum obtained from the measured matrix area, sampled away from the tissue, from the tissue spectrum. To asses delocalization, haematoxylin and eosin (H&E) were co-registered using the co-registration function in FlexImaging. The H&E and *m/z* images were exported as .Tiff files and loaded into ImageJ (Version 1.52a) and transformed to 8-bit grayscale, with 0 pixel intensity indicating no signal (i.e., black), and 255 pixel intensity indicating maximum signal (i.e., white). Tissue edges were determined from the co-registered H&E. Delocalization of tissue components was measured by creating line profiles showing the intensity distribution from the edge of the tissue onto the glass slide. Line profiles were created parallel to the scanning directions so that the distance away from the tissue where signal was detected could be accurately determined based on the number of pixels and the pixel size.

Accurate mass measurement profiling experiments were performed at random positions on the tissue using a 9.4 T Solarix Fourier transform ion cyclotron resonance (FT-ICR, Bruker Daltonik GmbH, Bremen, Germany) for lipid identification at the sum composition level. For each measurement position, 300 shots were accumulated. 4 million data points were collected resulting in a 2.936 s transient length and a mass resolution of 200,000 Full Width at Half Maximum (FWHM) at *m/z* 800. Sum-composition lipid identifications were made using a mass error tolerance of less than 1 ppm and assigned based on the lipid maps database (www.lipidmaps.org). Mass error calculations can be found in Supplementary Table 2.

Imaging measurements on the Solarix FT-ICR were performed in triplicate on consecutive sections at a 200 µm raster size, resulting in around 2800 pixels collected per tissue section. The mass range was set to the same values as for the rapifleX. For DHB, 200 shots per pixel were accumulated. For NRM, 200 shots per pixel were accumulated in positive ion mode and 150 shots in negative ion mode 1million data points were collected resulting in a 0.734 s transient length. Spectra were exported from Fleximaging as CSV files to Mmass [38] for peak picking to obtain information on the number of peaks and S/N per condition. The entire tissue was used for evaluation of the number of peaks and S/N, to prevent sampling bias. Peak picking settings in Mmass were set at a S/N threshold of 10, picking height set at 80% (in relation to the higher resolution) and both absolute and relative intensity threshold set at 0, no baseline correction or smoothing was performed. Matrix-related peaks were subtracted from the tissue spectrum by subtracting the spectrum obtained from the matrix area, sampled away from the tissue, from the tissue spectrum.

2.5. Tissue staining

After MSI, the matrix was washed from the tissue section by submersion in ethanol for 2 min and subsequent rehydration in water for

2 min. Slides were then submersed in haematoxylin for 3 min and eosin for 30 s with a 3 min tap water rinse step after each staining step for H& E staining. Slides were then submersed in ethanol for 1 min and xylene for 30 s prior to covering with entellan mounting medium and a cover slip. The H&E slides were scanned using a Mirax Desk Scanner (Zeiss, Gottingen, Germany).

3. Results and discussion

3.1. Evaluation of the sensitivity of chosen sample preparation methods

Matrix sublimation and matrix spraying were both capable of coating the samples with matrix in under 10 min using either NRM or DHB, while still providing high intensity signals. In the case of spraying, the limited number of layers did result in evaporation of the matrix from the coated slides in the high vacuum of the mass spectrometers within 90 min, which resulted in gradual loss of signal with time. In a clinical setting where a single section is expected to be analyzed within 10–20 min, depending on the sample size and resolution, this is not expected to be an issue. However, for large-scale studies with multiple sections on a single slide, the spraying methods we evaluated would be less suitable. Alternatively, less volatile matrices could be used [39].

Results between matrix spraying and sublimation were comparable for NRM in both positive and negative ionization mode with regard to number of peaks and average S/N levels (Fig. 1A and B, Table 1, Supplementary Fig. 2A and B). When the background matrix peaks were subtracted from the spectrum, more peaks were observed following matrix sublimation compared to matrix spraying (Supplementary Table 3). In addition, the variation in S/N was lower for sublimation compared to spraying (Table 1, Supplementary Table 3). The greater reproducibility for sublimation could potentially be attributed to the controlled environment in the sublimation chamber compared to the variable ambient conditions under which matrix spraying takes place [40]. In addition, the homogeneity of the matrix deposition after sublimation and the purity of sublimated matrix could also play a role in the reduced variation following matrix sublimation [28]. Variation was higher for NRM in negative ion mode, compared to positive ion mode, for all matrix deposition methods (Supplementary Table 1). Since all samples were first measured in positive ion mode before measuring in negative ion mode, it is possible that this variation resulted from evaporation of the matrix from the tissue sample due to the longer period in the vacuum of the instrument. Nevertheless, variation in the number of peaks detected was less than 10% for sublimation in negative ion mode.

Measurements at a 50 μm raster allowed clear separation between tissue types in both positive and negative ion mode. In positive ion mode, *m/z* 808.5 ($[PC\ 36:2 + Na]^+$) showed the highest relative abundance in the submucosa (Fig. 1C and E, Supplementary Fig. 3A) and 718.5 ($[PC\ O\text{-}32:1 + H]^+$) showed the highest relative abundance in the mucosa (Fig. 1D and E, Supplementary Fig. 3B). In negative ion mode, *m/z* 835.5 ($[PI\ 34:1 - H]^-$) was only detected in the mucosa (Supplementary Figs. 2C and E and 4A), whereas *m/z* 766.5 ($[PE\ 38:4 - H]^-$) highlighted the smooth muscle layers (Supplementary Fig. 2D and E and 4B).

With DHB, nearly twice the number of peaks were obtained from the matrix sublimation procedure versus matrix spraying by either of the tested methods (Fig. 2B), and average S/N levels for sublimation were also higher when measured on a TOF-MS instrument (Fig. 2A, Table 1). This effect was even more pronounced when the background matrix peaks were subtracted (Supplementary Table 3). Again, sublimation showed less variation in the number of peaks when compared to the spraying methods, although a similar low variation was observed between spraying and sublimation with regard to the average S/N levels (Fig. 2A and B, Supplementary Table 3). This difference is reflected in the images where *m/z* 853.6 ($[SM\ d42:1 + K]^+$) is detected in all samples, *m/z* 369.3 ($[Cholesterol\text{-}H_2O + H]^+$) was detected in the sublimated sample, but not in the sample sprayed with the SunCollect apparatus (Fig. 2C–E, Supplementary Fig. 5). Although *m/z* 369.3 was detected in the sample sprayed with the HTX, the signal was also present in the area with matrix only, suggesting a possible matrix-interference (Fig. 2D, left panel). It has recently been shown that cholesterol and vitamin E have a preference to migrate to the top of the matrix layer after matrix sublimation [30]. This could potentially explain the detection of cholesterol after sublimation in these samples. It is unclear why cholesterol was visible in the samples sprayed with the HTX but not in those sprayed with the SunCollect but it could potentially be due to the higher temperature from the HTX spraying resulting in a drier matrix deposition. In the sublimated sample, cholesterol was primarily detected in the mucosa, but also in the smooth muscle layer. Additionally, in the sample sprayed with the HTX, *m/z* 369.3 showed the highest relative abundance on tissue, (Supplementary Fig. 5B). The Solarix FT-ICR was able to resolve these peaks at 369.3512 ($[Cholesterol\text{-}H_2O + H]^+$; mass error −0.81 ppm) and 369.3564 showing that cholesterol can indeed be detected after spraying despite overlap of peaks in the Time-of-Flight (TOF) instruments. The highest intensity of *m/z* 853.6 showed showed in the smooth muscle and submucosal areas.

TOF instruments are most likely to be used in clinical imaging because of their high-throughput capability. However, the limited mass resolution of TOF mass spectrometers compared to Fourier Transform Mass Spectrometry (FT-MS) systems results in overlap of isobaric species. The overlap of different matrix-related and tissue-related peaks in TOF instruments can lead to misinterpretation of the number of unique *m/z* values generated for different matrix application methods. Therefore, evaluation of the number of peaks and S/N was also performed using an FT-ICR. Although direct comparison between the TOF-MS and FT-ICR MS is difficult due to differences in source pressure, analyzers, and peak picking settings, the FT-ICR provides a more accurate representation of the unique *m/z* values for the different methods compared to the TOF-MS. Overall, the Solarix FT-ICR produced more reproducible results compared to the rapifleX. This could partly be attributed to: i) the fact that the Solarix is less susceptible to height differences due to the larger laser spot size and depth of focus; and ii) the decoupling of the ionization and mass analysis. In addition, the different source pressure for the rapifleX and Solarix can result in different matrix adduct formation and in-source fragmentation of analytes, which could explain the difference in detected peaks. For NRM, more peaks were obtained with sublimation compared to spraying in both positive and negative ion modes, particularly after subtraction of matrix-related peaks (Table 2, Supplementary Table 4 and Fig. 6A–D). S/N was comparable between all three matrix application methods for NRM. For DHB, a similar numbers of peaks was detected after either

Table 1
Comparison of S/N *and number of peaks (n = 3).*

DHB		
positive ion mode	average S/N (RSD)	Number of peaks (RSD)
TM-sprayer	33 (6.6%)	195 (22.8%)
SunCollect	34 (92%)	212 (22.2%)
Sublimation	72 (8.0%)	383 (12.0%)
NRM		
positive ion mode		
TM-sprayer	80 (12.8%)	441 (19.1%)
SunCollect	69 (16.3%)	405 (3.0%)
Sublimation	93 (3.8%)	489 (5.4%)
negative ion mode		
TM-sprayer	59 (8.7%)	281 (14.6%)
SunCollect	58 (5.2%)	221 (13.8%)
Sublimation	74 (9.0%)	267 (5.7%)

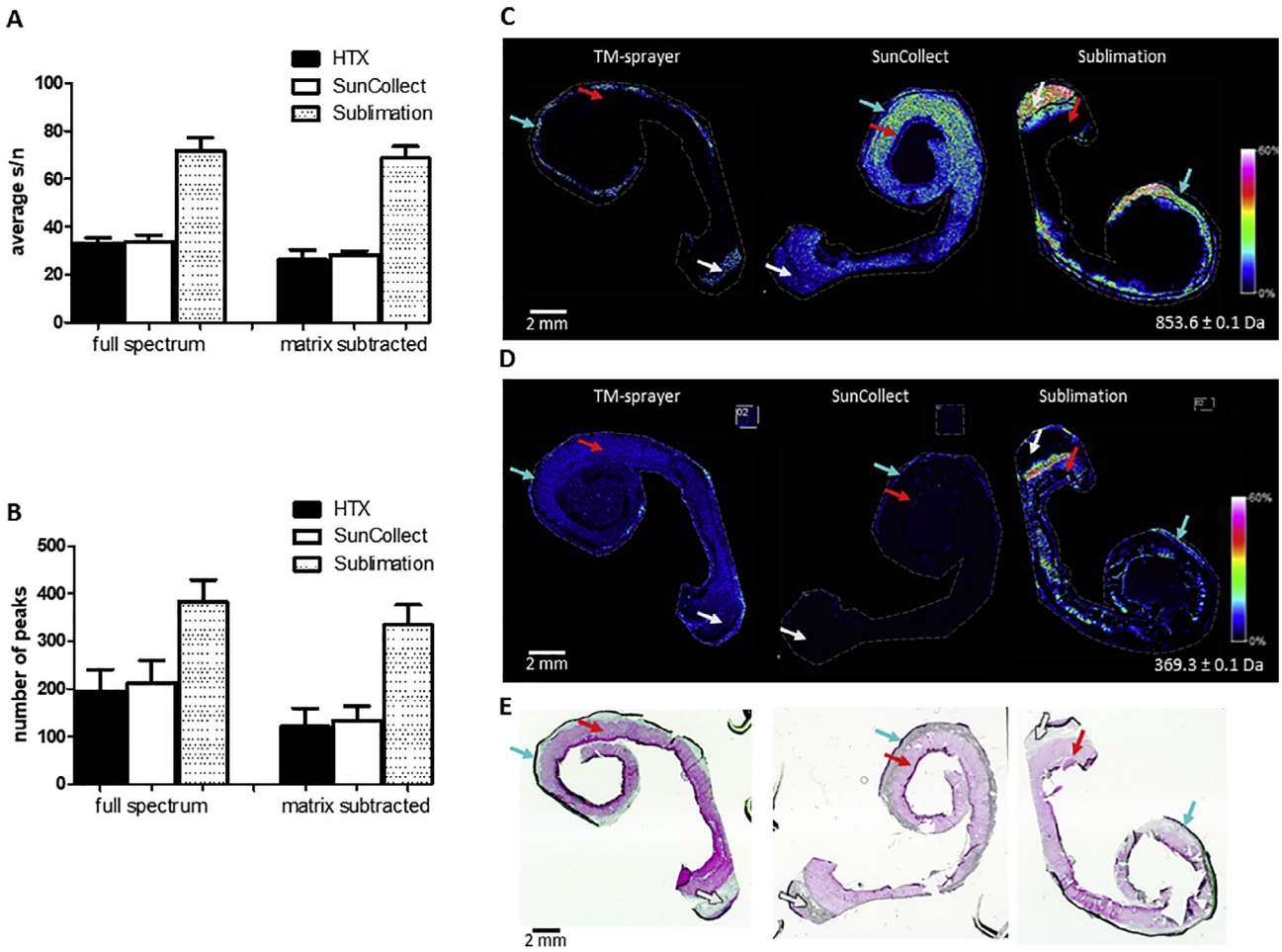

Fig. 2. Signal intensity (A, C, D) and detected peaks (B) in positive ion mode matrix application of DHB. (A) Average S/N obtained after matrix application using HTX, SunCollect or sublimation for the full spectrum (left bars) or after matrix peaks were subtracted (right bars). Error bars represent standard deviation (n = 3). (B) Mean number of peaks obtained after matrix application using HTX, SunCollect or sublimation for the full spectrum (left bars) or after matrix peak were subtracted (right bars). Error bars represent standard deviation (n = 3). (C) Ion intensity distribution at 50 um raster size of *m/z* 853.6 ± 0.1 Da ($[SM\ d42{:}1 + K]^+$) and (D) 369.3 ± 0.1 Da ($[Cholesterol - H_2O + H]^+$). Images were normalized to TIC. (E) H&E stain of the measured tissues corresponding to the images in C and D. Arrows show mucosa (blue), submucosa (white), and muscle (red) on H&E and corresponding location in the *m/z* images.

Table 2
Comparison of S/N and number of peaks obtained on FT-ICR (n = 3).

DHB		
positive ion mode	average S/N (RSD)	Number of peaks (RSD)
TM-sprayer	708 (2.1%)	2610 (8.9%)
SunCollect	603 (12.6%)	1908 (3.0%)
Sublimation	1153 (20.8%)	2558 (3.8%)
NRM		
positive ion mode		
TM-sprayer	1954 (4.0%)	2832 (3.5%)
SunCollect	2311 (21.2%)	2733 (3.4%)
Sublimation	1980 (18.1%)	4040 (4.8%)
negative ion mode		
TM-sprayer	629 (13.8%)	2304 (7.0%)
SunCollect	544 (2.3%)	2328 (4.6%)
Sublimation	560 (6.7%)	2826 (8.3%)

spraying or sublimation. Average S/N was higher for sublimation than spraying, but the variation was also higher for the sublimated samples compared to the sprayed samples (Table 2, Supplementary Table 4 and Fig. 6E and F).

Although FT-ICR systems provide a more accurate representation of the detected unique *m/z* values, the longer measurement time required to obtain ultrahigh molecular resolution datasets makes these instruments less suitable for routine high-throughput clinical diagnostics. In addition, the longer measurement time on high resolution instruments puts less pressure on sample preparation time, thus allowing optimization of the spraying methods with regards to reproducibility and extraction efficiency for specific molecule classes. In this regard, spraying methods offer more flexibility towards specific, targeted, uses by changing solvent composition and spray wetness compared to sublimation.

3.2. Evaluation of delocalization

At a 10 μm raster size, clear spatial features within the tissue could be discerned (Fig. 3). Signal was observed outside of the tissue, representative of delocalization, for NRM at 50 μm distance for sublimation and 120–160 μm distance for spraying, and for DHB at around 80–120 μm for spraying and 60–70 μm for sublimation (Supplementary Figs. 7 and 9). This observed delocalization can be partially attributed to folding of the tissue caused by the extensive washing of the sample required for staining (Supplementary Fig. 8). In addition, condensation from moisture that formed on the sample during transport from the

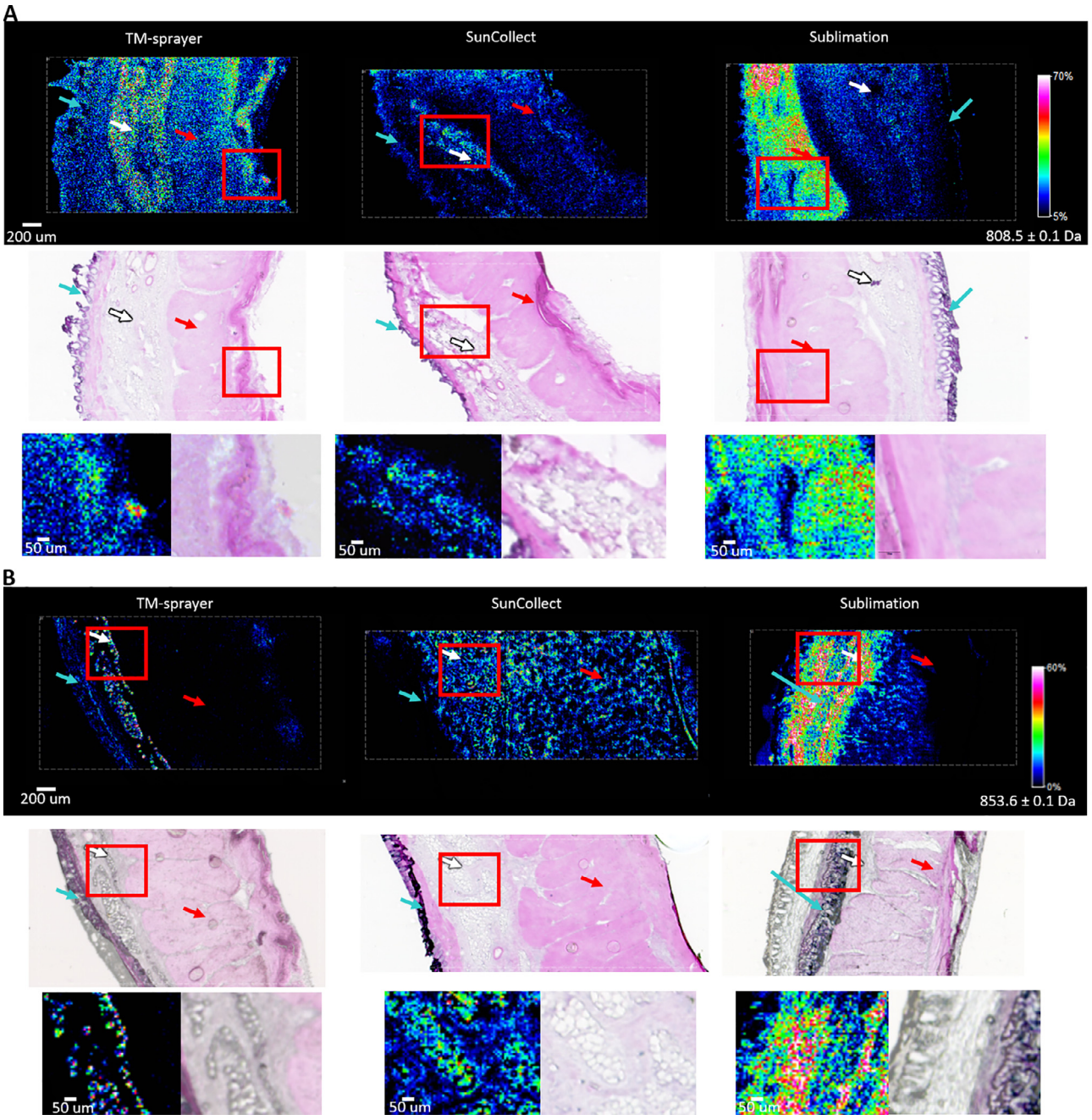

Fig. 3. 10 μm raster size MALDI-MSI image with corresponding H&E stain. (A) Ion intensity distribution at 10 μm of *m/z* 808.5 ± 0.1 ($[PC\ 36:2 + Na]^+$) after application of NRM using HTX (left), SunCollect (middle) or sublimation (right) with corresponding H&E stain. Images were normalized to TIC (B) Ion intensity distribution at 10 μm of *m/z* 853.6 ± 0.1 ($[SM\ d42:1 + K]^+$) after application of DHB using HTX (left), SunCollect (middle) or sublimation (right) with corresponding H&E stain. Images were normalized to TIC. Arrows show mucosa (blue), submucosa (white), and muscle (red) on H&E and corresponding location in the *m/z* images. Bottom panels in (A) and (B) are zoomed in images of the region marked with the red square.

−80 °C storage freezer to the desiccator could have contributed to delocalization; this is mostly relevant for the edge of the tissue, whereas the bulk of tissue is generally less affected by this effect. Although all three matrix application devices allowed discernment of distinct spatial features in the tissue, imaging at a 10 μm raster size will not be routinely performed for clinical diagnostics due to the time required to obtain a 10 μm image (45 min) versus a 50 μm image (2 min). However, while the translation of MSI to routine molecular pathology will involve high throughput screening techniques, including 50 μm raster imaging, there will be times when high spatial molecular resolution (i.e., 10 μm raster) MSI or profiling techniques will be useful, or needed.

3.3. Effect of omitting sample desiccation step

A significant time sink in sample preparation is desiccation, which generally takes 20 min. Desiccation is usually done to prevent moisture in the sample from causing delocalization when the sample is transferred from frozen conditions, such as the −80 °C freezer or the microtome, to room temperature. Since the vacuum of the sublimation device acts as a desiccator, we tested whether it would be possible to remove the desiccation step from the sublimation workflow directly after tissue sectioning and achieve similar results. To similarly shorten the desiccation time we implemented a step in the spray-based workflow where the sample was rapidly desiccated using a nitrogen gas flow.

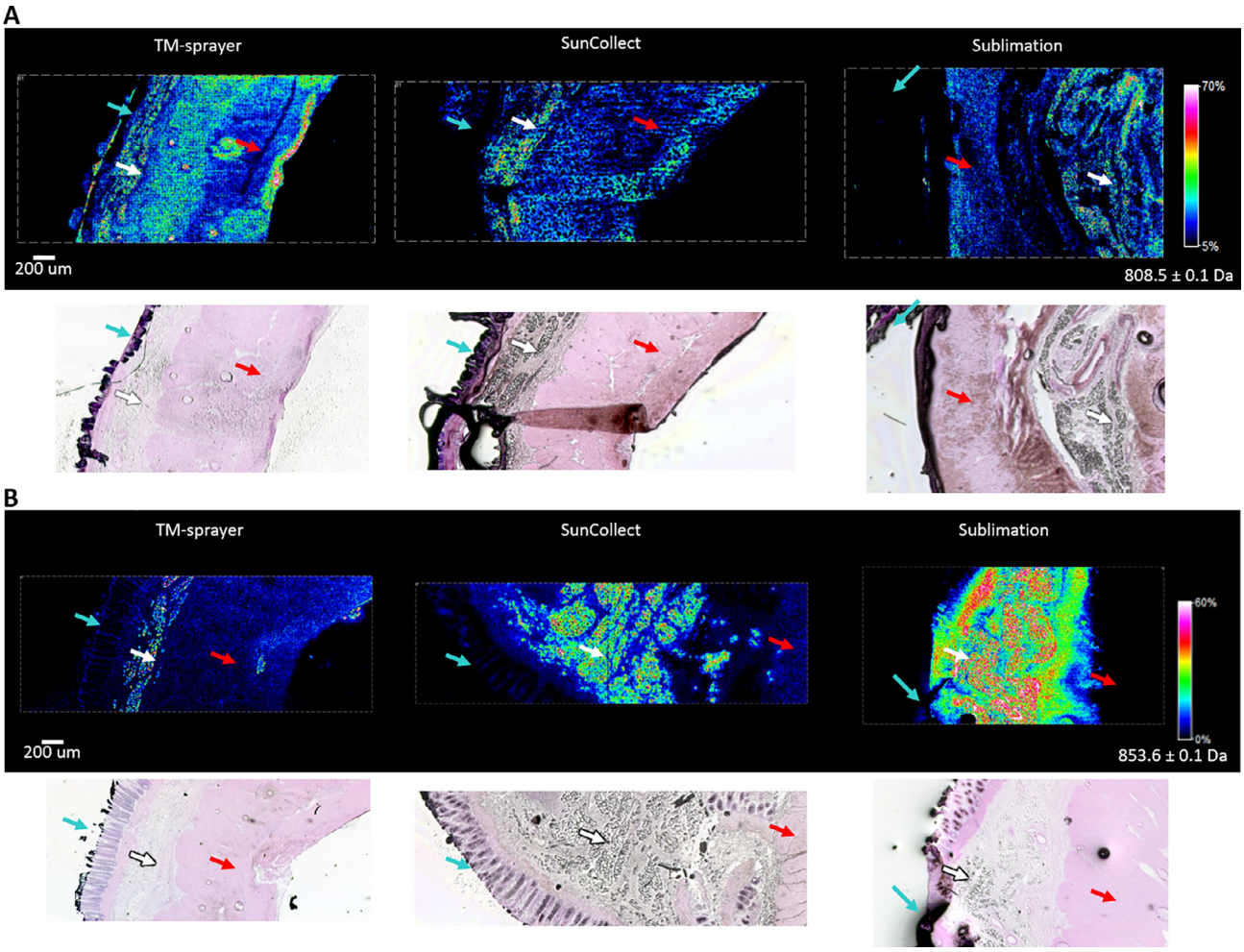

Fig. 4. 10 μm resolution MALDI-MSI image when desiccation was omitted prior to matrix application with corresponding H&E stain. (A) Ion intensity distribution at 10 μm of *m/z* 808.5 ± 0.1 ([PC 36:2 + Na]$^+$) after application of NRM using HTX (left), SunCollect (middle) or sublimation (right) with corresponding H&E stain. Images were normalized to TIC (B) Ion intensity distribution at 10 μm of *m/z* 853.6 ± 0.1 ([SM d42:1 + K]$^+$) after application of DHB using HTX (left), SunCollect (middle) or sublimation (right) with corresponding H&E stain. Images were normalized to TIC. Arrows show mucosa (blue), submucosa (white), and muscle (red) on H&E and corresponding location in the *m/z* images.

No delocalization was observed for 10 μm raster size images for NRM for both the sprayed and the sublimated sample (Fig. 4A, Supplementary Figs. 10A and 11). For DHB, no delocalization was observed for either sublimation or SunCollect matrix applications up to 90 μm from the tissue with the TM-sprayer (Fig. 4B, Supplementary Figs. 10B and 11) coated samples using these approaches.

The absence of delocalization, when desiccation was omitted or by using the flowing nitrogen for desiccation in comparison to samples that were desiccated in the vacuum desiccator, can be explained by the fact that these samples were taken directly from the microtome to the sample preparation devices to more accurately simulate the clinical situation, preventing any ice and subsequent condensation occurring from storage in the −80 °C freezer.

Care should be taken though, especially with regards to spraying, of the ambient conditions in the laboratory when omitting the vacuum desiccation step and drying with flowing nitrogen gas instead as severe delocalization can occur upon spraying. This effect is mostly prevented with sublimation since it is a controlled vacuum environment, although in modern sprayers the environmental humidity effect is also greatly reduced owing to the constant flow of nitrogen creating a positive nitrogen rich atmosphere within the sprayer compartment. In addition, the use of closed, dry, boxes for the transportation of samples could aid the prevention of condensation causing delocalization.

3.4. Clinical workflow

The entire workflow, including transfer to the different devices, was timed to evaluate if it would meet a clinical diagnostic timeline of less than 30 min. Under optimal conditions, sample preparation (i.e., microtome cutting and matrix application) required 9 min when applying matrix by sublimation and 10 min for spraying. Another 5 min was required to set up the imaging run, which included an optical scan of the section, entering coordinates into the instrument and calibration of the instrument. To meet our timeline, 15 min remain for imaging, which would allow analysis of a 1.13 cm^2 tissue section at a 50 μm raster or a 4.5 cm^2 tissue section at 100 μm raster (Fig. 5).

For the application of matrix by sublimation, the matrix was dissolved in acetone prior to placing it on the heating plate and the mixture was allowed to evaporate, leaving crystallized matrix. This facilitated even spreading of the matrix over the heating element and created close contact between the heating element and the matrix. This close contact enabled efficient heat transfer in the vacuum chamber being used for the sublimation process, and, thereby, increased throughput and reproducibility.

From a practical point of view, the preparation steps for sublimation application are simpler and less time consuming than those for spraying since no extensive sonication is needed to fully dissolve the matrix in the solvent. Additionally, the solution-based degradation of DHB over

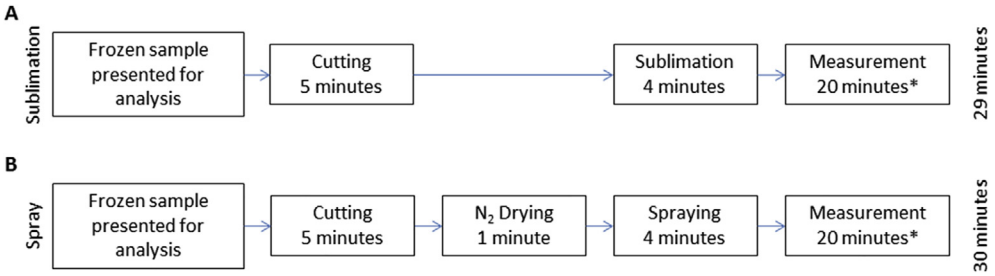

Fig. 5. Optimized workflow for MALDI-MSI for sublimation (A) and spraying (B) with time necessary per step including transfer time between steps. *Measurement time is dependent on sample size and imaging resolution.

time, which has been reported to cause significant changes within a week [41], is eliminated with sublimation. In contrast, methods for spraying have been more extensively reported and most labs have more experience with automated sprayers. Hence, standard protocols can be more readily integrated with matrix spraying systems. Sprayers offer broad flexibility in the method of sample preparation used, thereby allowing for facile switching of the analyte profile targeted by changing solvent composition; this is not the case with sublimation alone. Continuous advances in spraying technology also increase the potential for spraying to compete as an adequately rapid sample preparation technique. However, automated sublimation devices are now commercially available (e.g., iMLayer, Shimadzu, Kyoto, Japan) and the current sublimation set-up developed for this publication is fully software controlled, thus automated protocols can begin to be incorporated for different applications for sublimation. Sprayers, however, are able to coat multiple tissue sections, simultaneously, whereas the current iteration of our sublimation setup can only coat one sample at a time. However, simple modifications of our device would also allow for the simultaneous coating of multiple slides. A benefit of this protocol is an increased level of standardization and robustness, combined with a relatively easy process for method development and automation, which may contribute to a greater understanding of the value of sublimation for routine screening purposes in the clinic.

4. Conclusion

This work demonstrates that matrix application to tissue samples for MALDI-MSI using either spraying or sublimation protocols can result in reproducible results for analysis within a clinical time frame while maintaining adequate sensitivity and spatial resolution.

While sublimation offers the advantage of a straightforward robust sample preparation method under controlled ambient conditions that reduces the risk of analyte delocalization, spraying offers the ability to fine tune the method for targeted analysis by changing solvent composition and spray settings. Therefore, even though sublimation provided slightly better results with DHB, it is likely that spray settings could be optimized to provide similar sensitivity. In addition, sprayers have been commercially available for a considerable time and ongoing development continues to improve their performance.

While evaluation of two matrix spray methods and an in-house developed sublimation method was an important component of this work, more important was our demonstration that these methods can fit within a MALDI-MSI designed for clinical use. We were able to demonstrate that a MALDI-MSI workflow of less than 30 min is achievable for sample sizes that correspond to an average clinical biopsy size. The approaches described here provide the groundwork towards integration of MSI in routine molecular pathology for clinical diagnostics.

Acknowledgments

This research was made possible with the financial support of the LINK program of the Dutch Province of Limburg. The matrix sublimation development was supported by an Enabling Technologies B.V valorization project. F.P.Y.B. received funding from the European Union's Horizon 2020 research and innovation program under the Marie Sklodowska-Curie Program, TargetCare (ITN-2014-ETN 642414). We gratefully acknowledge support of Janssen R&D (Beerse, Belgium).

Conflict of interest statement

LRS Huizing has a patent Sample preparation device pending; BWAMM Beulen reports Grants from Enabling Technologies, Grants from NWO KIEM, during the conduct of the study; In addition, Dr. Beulen has a patent on matrix sublimation technology. S.R. Ellis has a patent Sample preparation device pending. FPY Barré reports other funding from HTX Imaging, during the conduct of the study; PB Kwant reports a patent Sample Preparation Apparatus pending with royalties received from HTX Imaging BV, and a patent null pending. RJ Vreeken has nothing to disclose; RMA Heeren reports grants from Province of Limburg, during the conduct of the study; In addition, RMA. Heeren has a patent Sample preparation device pending.

Appendix A. Supplementary data

Supplementary data to this article can be found online at https://doi.org/10.1016/j.clinms.2019.01.004.

References

[1] B.M. Gruner, et al., Modeling therapy response and spatial tissue distribution of Erlotinib in pancreatic cancer, Mol. Cancer Ther. 15 (5) (2016) 1145–1152.
[2] S. Lou, et al., High-grade sarcoma diagnosis and prognosis: biomarker discovery by mass spectrometry imaging, Proteomics 16 (11–12) (2016) 1802–1813.
[3] K. Scupakova, et al., Spatial systems lipidomics reveals nonalcoholic fatty liver disease heterogeneity, Anal. Chem. 90 (8) (2018) 5130–5138.
[4] P.-M. Vaysse, et al., Mass spectrometry imaging for clinical research – latest developments, applications, and current limitations, Analyst 142 (15) (2017) 2690–2712.
[5] L.M. Cole, M.R. Clench, Mass spectrometry imaging tools in oncology, Biomark. Med. 9 (9) (2015) 863–868.
[6] L. Jiang, et al., MALDI-mass spectrometric imaging revealing hypoxia-driven lipids and proteins in a breast tumor model, Anal. Chem. 87 (12) (2015) 5947–5956.
[7] J. Depreeuw, et al., Characterization of patient-derived tumor xenograft models of endometrial cancer for preclinical evaluation of targeted therapies, Gynecol. Oncol. 139 (1) (2015) 118–126.
[8] A. Ly, et al., High-mass-resolution MALDI mass spectrometry imaging of metabolites from formalin-fixed paraffin-embedded tissue, Nat. Protoc. 11 (8) (2016) 1428–1443.
[9] Y. Sugihara, et al., Laser microdissection and two-dimensional difference gel electrophoresis reveal proteomic intra-tumor heterogeneity in colorectal cancer, J. Proteomics 78 (2013) 134–147.
[10] B. Balluff, M. Hanselmann, R.M. Heeren, Mass Spectrometry Imaging for the Investigation of Intratumor Heterogeneity, Adv. Cancer Res. 134 (2017) 201–230.
[11] J.A. Barry, et al., Assessing drug and metabolite detection in liver tissue by UV-MALDI and IR-MALDESI mass spectrometry imaging coupled to FT-ICR MS, Int. J. Mass Spectrom. 377 (2015) 448–1155.
[12] L. Carlred, et al., Imaging of amyloid-β in Alzheimer's disease transgenic mouse brains with ToF-SIMS using immunoliposomes, Biointerphases 11 (2) (2016) 02A312.
[13] M. Sugimoto, et al., Histological analyses by matrix-assisted laser desorption/ionization-imaging mass spectrometry reveal differential localization of sphingomyelin molecular species regulated by particular ceramide synthase in mouse

brains, Biochim. Biophys. Acta, Proteins Proteomics 1851 (12) (2015) 1554–1565.
[14] A. Likos, et al., Local mosquito-borne transmission of Zika Virus – Miami-Dade and Broward Counties, Florida, June-August 2016, MMWR Morb. Mortal. Wkly Rep. 65 (38) (2016) 1032–1038.
[15] N. Ogrinc Potocnik, et al., Use of advantageous, volatile matrices enabled by next-generation high-speed matrix-assisted laser desorption/ionization time-of-flight imaging employing a scanning laser beam, Rapid Commun. Mass Spectrom. 29 (23) (2015) 2195–2203.
[16] J.M. Spraggins, R.M. Caprioli, High-speed MALDI-TOF imaging mass spectrometry: rapid ion image acquisition and considerations for next generation instrumentation, J. Am. Soc. Mass Spectrom. 22 (6) (2011) 1022–1031.
[17] F. Barré, et al., Faster raster matrix-assisted laser desorption/ionization mass spectrometry imaging of lipids at high lateral resolution, Int. J. Mass Spectrom. (2018).
[18] R.J. Goodwin, Sample preparation for mass spectrometry imaging: small mistakes can lead to big consequences, J. Proteomics 75 (16) (2012) 4893–4911.
[19] R.M.R. Caprioli, Molecular imaging of biological samples: localization of peptides and proteins using MALDI-TOF MS, Anal. Chem. 69 (23) (1997) 4751–4760.
[20] A. Römpp, et al., Mass spectrometry imaging with high resolution in mass and space (HR2 MSI) for reliable investigation of drug compound distributions on the cellular level, Anal. Bioanal. Chem. 401 (1) (2011) 65–73.
[21] K. Börner, et al., Molecular imaging of lipids in cells and tissues, Int. J. Mass Spectrom. 260 (2–3) (2007) 128–136.
[22] R. Ceuppens, et al., Direct profiling of myelinated and demyelinated regions in mouse brain by imaging mass spectrometry, Int. J. Mass Spectrom. 260 (2–3) (2007) 185–194.
[23] T.W. Jaskolla, et al., Comparison between vacuum sublimed matrices and conventional dried droplet preparation in MALDI-TOF mass spectrometry, J. Am. Soc. Mass Spectrom. 20 (6) (2009) 1104–1114.
[24] E. Gemperline, S. Rawson, L. Li, Optimization and comparison of multiple MALDI matrix application methods for small molecule mass spectrometric imaging, Anal. Chem. 86 (20) (2014) 10030–10035.
[25] H. Kettling, et al., MALDI mass spectrometry imaging of bioactive lipids in mouse brain with a Synapt G2-S mass spectrometer operated at elevated pressure: improving the analytical sensitivity and the lateral resolution to ten micrometers, Anal. Chem. 86 (15) (2014) 7798–7805.
[26] A. Nilsson, et al., Mass Spectrometry Imaging proves differential absorption profiles of well-characterised permeability markers along the crypt-villus axis, Sci. Rep. 7 (1) (2017) 6352.
[27] A. Zavalin, et al., Tissue protein imaging at 1 mum laser spot diameter for high spatial resolution and high imaging speed using transmission geometry MALDI TOF MS, Anal. Bioanal. Chem. 407 (8) (2015) 2337–2342.
[28] J.A. Hankin, R.M. Barkley, R.C. Murphy, Sublimation as a method of matrix application for mass spectrometric imaging, J. Am. Soc. Mass Spectrom. 18 (9) (2007) 1646–1652.
[29] A. Ly, et al., High-resolution MALDI mass spectrometric imaging of lipids in the mammalian retina, Histochem. Cell Biol. 143 (5) (2015) 453–462.
[30] S. Van Nuffel, et al., Insights into the MALDI process after matrix deposition by sublimation using 3D ToF-SIMS imaging, Anal. Chem. 90 (3) (2018) 1907–1914.
[31] A. Thomas, et al., Sublimation of new matrix candidates for high spatial resolution imaging mass spectrometry of lipids: enhanced information in both positive and negative polarities after 1,5-diaminonapthalene deposition, Anal. Chem. 84 (4) (2012) 2048–2054.
[32] D.M. Anderson, et al., High spatial resolution imaging mass spectrometry of human optic nerve lipids and proteins, J. Am. Soc. Mass Spectrom. 26 (6) (2015) 940–947.
[33] M.B. O'Rourke, et al., A versatile cost-effective method for the analysis of fresh frozen tissue sections via matrix-assisted laser desorption/ionisation imaging mass spectrometry, Rapid Commun. Mass Spectrom. 29 (7) (2015) 637–644.
[34] J. Yang, R.M. Caprioli, Matrix sublimation/recrystallization for imaging proteins by mass spectrometry at high spatial resolution, Anal. Chem. 83 (14) (2011) 5728–5734.
[35] S. Shimma, et al., Alternative two-step matrix application method for imaging mass spectrometry to avoid tissue shrinkage and improve ionization efficiency, J. Mass Spectrom. 48 (12) (2013) 1285–1290.
[36] RICHTLIJNEN VOOR AANVRAGEN EN INZENDEN PATHOLOGIE ONDERZOEK. 2018 [cited 2018 20-12-2018]; 16:[Guideline to pathology material handling]. Available from: https://webshare.iprova.nl/lzhjmgw71wz3zltb/Document.aspx.
[37] D.A. Novis, R.J. Zarbo, Interinstitutional comparison of frozen section turnaround time. A College of American Pathologists Q-Probes study of 32868 frozen sections in 700 hospitals, Arch. Pathol. Lab. Med. 121 (6) (1997) 559–567.
[38] M. Strohalm, mMass data miner: an open source alternative for mass spectrometric data analysis, Rapid Commun. Mass Spectrom. 22 (6) (2008) 905–908.
[39] J. Yang, J.L. Norris, R. Caprioli, Novel vacuum stable ketone-based matrices for high spatial resolution MALDI imaging mass spectrometry, J. Mass Spectrom. 53 (10) (2018) 1005–1012.
[40] Y.-M. Ou, et al., Preparation of homogeneous MALDI samples for quantitative applications, JoVE 116 (2016) e54409.
[41] J. Schiller, et al., The suitability of different DHB isomers as matrices for the MALDI-TOF MS analysis of phospholipids: which isomer for what purpose? Eur. Biophys. J. 36 (4–5) (2007) 517–527.